pp 1606–1629. © Royal Aeronautical Society 2018
doi: 10.1017/aer.2018.93

Aeroelastic modelling and stability analysis of tiltrotor aircraft in conversion flight

Z. Li and P. Xia
xiapq@nuaa.edu.cn
National Key Laboratory of Rotorcraft Aeromechanics
College of Aerospace Engineering
Nanjing University of Aeronautics and Astronautics
Nanjing, China

ABSTRACT

In conversion flight, the aeroelastic modelling of tiltrotor aircraft needs to consider the unsteady effect of the rotor wake bending due to the rotor tilting. In this paper, the unsteady models of the rotor wake bending and dynamic inflow have been introduced into the aeroelastic modelling of the tiltrotor aircraft in conversion flight by using Hamilton's generalized principle. The method for solving the aeroelastic stability of tiltrotor aircraft in conversion flight has been established by using the small perturbation theory and the Floquet theory. The influences of unsteady dynamic inflow on trim control inputs and aeroelastic stability of a tiltrotor aircraft in conversion flight were calculated and analysed. The calculation results show that the required collective pitch increases with the pylon tilting forward and the unsteady inflow is trimmed primarily by the lateral cyclic pitch of the rotor. The wake bending unsteady dynamic inflow can obviously reduce the stability of the flapping modes of the rotor, and have no obvious influence on the lag modes of the rotor and the motion modes of the wing. The instability of tiltrotor occurs in the chordwise bending mode of the wing when the pylon tilts to a certain angle in high speed forward flight.

Keywords: Tiltrotor aircraft; conversion flight; aeroelastic stability; rotor wake bending; dynamic inflow; unsteady aerodynamic forces

Received 29 September 2017; revised 7 June 2018; accepted 29 June 2018.

NOMENCLATURE

c	chord length of blade
C_d	drag coefficient of the aerofoil
$C_{l\alpha}$	lift curve slope of blade
$\mathbf{C}_{pk}$	inflow coupling matrix of wake bending
C_T, C_H, C_Y, C_Q	thrust, backward, sideward forces and torque coefficients of rotor
h	pylon length
$\tilde{L}$	gain matrix relating to the skew angle-of-wake
m_s	the blade mass per unit length
m_w	the wing mass per unit length
m_p	the mass of pylon
$\mathbf{M}$	mass matrix in inflow state equations
M_{tip}	Mach number of blade tip
N_b	number of blade
q	dynamic pressure
q_h, p_h	longitudinal and lateral tilting angular velocity of pylon
$\overline{r}$	dimensionless radius of blade
x_p, y_p, z_p	translational deformation degrees of freedom of wing tip
V	forward speed (forward speed $V/\Omega R$)
$\overline{V_c}$	the component of forward speed along pylon
$\mathbf{V}$	mass flow parameter matrix
w_{bi}	normal velocity caused by blade motion
α_p	tilt angle-of-pylon
α_x, α_y, α_z	rotational deformation degrees of freedom of wing tip
α_j^k, β_j^k	state variables of induced inflow
β, ξ	flapping and lag angle-of-blade
γ	Lock number of blade
θ_0, θ_c, θ_s	collective, longitudinal and lateral pitch
κ'	wake bending influence coefficient
λ_w	vertical induced inflow velocity on the rotor disk
ϕ	radial expand function
ψ	azimuth angle
ω_p, $\dot{\omega}_p$	tilting angular velocity and acceleration of pylon

1.0 INTRODUCTION

Tiltrotor aircraft has the flight capabilities of a helicopter and turboprop aircraft. The conversion flight between helicopter and turboprop aircraft can be achieved through by tilting the rotor pylon forward. While the pylon is in motion, the tilting rotor is in an unsteady aerodynamic environment and the rotor wake is undergoing bending, which makes the aeroelastic model of tiltrotor aircraft very complicated. Until now, the research on the dynamic stability of the tiltrotor aircraft has been mainly focused on the aeroelastic stability analysis in forward flight[1,2]. Active and passive control methods[3,4], like wing-flaperon and winglet, aeroelastically tailored blades[5] and composite wings[6,7] were used to improve the maximum forward flight speed of tiltrotor aircraft. A more accurate rotor inflow model is needed to assess the effects of rotor wake bending while the pylon is undergoing conversion.

https://doi.org/10.1017/aer.2018.93 Published online by Cambridge University Press

The Peters–He generalized dynamic inflow theory[8] takes into account the computational efficiency and accuracy, and has been applied in modelling of aeroelastic stability analysis for helicopters[9–11]. The author thoroughly studied the dynamic inflow modelling and aeroelastic responses of a rotor undergoing tilting motion[12], as well as the pylon whirl flutter and the divergent motion of wing of tiltrotor aircraft in forward flight[13]. On this basis, combing the rotor wake bending unsteady dynamic inflow model[12], the unsteady aerodynamic model[14,15] and the consideration of structural coupling of rotor/pylon/wing, the nonlinear aeroelastic model of tiltrotor aircraft in conversion flight has been presented in this paper, and the rotor/pylon/wing aeroelastic stability of a tiltrotor aircraft in different flight conditions was calculated and analysed.

2.0 AEROELASTIC MODELLING OF TILTROTOR AIRCRAFT IN CONVERSION FLIGHT

2.1 Dynamic modelling of tiltrotor aircraft

Figure 1 shows the structural dynamic model of a tiltrotor aircraft in conversion flight used in this paper. A rigid-body pylon which can tilt forward and backward about the pivot point is connected to one end of the articulated rotor system, while the other end is mounted at the elastic wing tip (point P). α_p is the tilt angle-of-pylon. The tiltrotor aircraft is in helicopter flight mode when the tilt angle is 0°, and in turboprop aircraft flight mode when the angle is 90°. ω_p is the tilting angular velocity of pylon. The wing tip degrees of freedom contain three translational degrees of freedom x_p, y_p, z_p and three rotational degrees of freedom α_x, α_y, α_z. h represents the distance between the hub and the pivot point. The first-order modes of global flapping β_0, β_{1c}, β_{1s} and global lag ξ_0, ξ_{1c}, ξ_{1s} are considered in this paper. The wing of the tiltrotor aircraft is treated as a cantilever beam with concentrated mass installed at end of the beam. The rotor system, wing and pylon constitute a coupled dynamic structural system by structural and motion coupling. The rotor aerodynamic forces and moments are shown in Fig. 1, where T, H, Y and Q are thrust, backward force, sideward force and torque of rotor, respectively (the dimensionless forms are C_T, C_H, C_Y and C_Q). Based on Hamilton's generalized principle, fully considering the couplings among rotor, pylon and wing of tiltrotor,

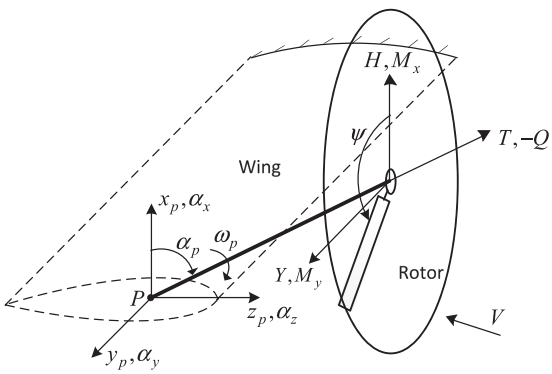

Figure 1. Structural dynamic model of tiltrotor aircraft in conversion flight.

https://doi.org/10.1017/aer.2018.93 Published online by Cambridge University Press

the equation for a non-conservative system is expressed as

$$\delta\Pi = \int_{t_1}^{t_2} (\delta U - \delta T - \delta W)\mathrm{d}t = 0 \quad \cdots(1)$$

where δU, δT and δW are the variations of the elastic strain energy, the kinetic energy and the work done by non-conservative forces, respectively. The contributions to these energy expressions from the blades and wing can be summed as

$$\delta U = \left(\sum_{1}^{N_b} \delta U_b\right) + \delta U_W \quad \cdots(2)$$

$$\delta T = \left(\sum_{1}^{N_b} \delta T_b\right) + \delta T_W \quad \cdots(3)$$

$$\delta W = \left(\sum_{1}^{N_b} \delta W_b\right) + \delta W_W \quad \cdots(4)$$

where the subscript b refers to the blade, W to the wing and N_b to the number of blades. The followings are the derivations of the energy terms of wing and rotor.

2.2 Dynamic modelling of rotor

According to the positional relationships of each component shown in Fig. 1 and supposing the blade is rigid, the position vector $\boldsymbol{R}$ in inertial co-ordinate system of an arbitrary point on the cross-section at radius r of the ith blade can be expressed as

$$\begin{aligned}
R_x &= r\cos\alpha_p\cos\psi + h\sin\alpha_p + r\beta\sin\alpha_p + r\xi\cos\alpha_p\sin\psi + r\alpha_x\sin\alpha_p\sin\psi + h\alpha_y\cos\alpha_p \\
&\quad - r\alpha_y\sin\alpha_p\cos\psi - r\alpha_z\sin\psi - r\xi\alpha_x\sin\alpha_p\cos\psi + r\beta\alpha_y\cos\alpha_p \\
&\quad - r\xi\alpha_y\sin\alpha_p\sin\psi + r\xi\alpha_z\cos\psi + x_p \\
R_y &= r\sin\psi - r\xi\cos\psi - h\alpha_x + r\alpha_z\cos\alpha_p\cos\psi - r\beta\alpha_x + h\alpha_z\sin\alpha_p + r\beta\alpha_z\sin\alpha_p \\
&\quad + r\xi\alpha_z\cos\alpha_p\sin\psi + y_p \\
R_z &= h\cos\alpha_p - r\sin\alpha_p\cos\psi + r\beta\cos\alpha_p - r\xi\sin\alpha_p\sin\psi + r\alpha_x\cos\alpha_p\sin\psi \\
&\quad - r\alpha_y\cos\alpha_p\cos\psi - h\alpha_y\sin\alpha_p + z_p - r\xi\alpha_x\cos\alpha_p\cos\psi - r\beta\alpha_y\sin\alpha_p - r\xi\alpha_y\cos\alpha_p\sin\psi \cdots(5)
\end{aligned}$$

where ψ is the azimuth angle, β and ξ are the flapping and the lag angle-of-blade, respectively. The flapping and lag motions of a single blade are transformed into the global flapping and lag motions of rotor by using the Fourier transformation[16], which are

$$\beta = \beta_0 + \beta_{1c}\cos\psi + \beta_{1s}\sin\psi \quad \cdots(6)$$

$$\xi = \xi_0 + \xi_{1c}\cos\psi + \xi_{1s}\sin\psi \quad \cdots(7)$$

The velocity of the point is determined by taking the time derivative of the position vector (5) and is given as

$$\boldsymbol{V}_b = \frac{\partial \boldsymbol{R}}{\partial t} \quad \cdots(8)$$

https://doi.org/10.1017/aer.2018.93 Published online by Cambridge University Press

The virtual kinetic energy variation of the ith blade is given by

$$\delta T_b = \int_0^R m_s \boldsymbol{V}_b \cdot \delta \boldsymbol{V}_b dr \qquad \cdots(9)$$

where m_s is the blade mass per unit length, R is the blade radius.

According to the description of rigid body kinematics, the virtual strain energy of the rotor is given by

$$\delta U_b = K_\beta \beta \delta\beta + K_\xi \xi \delta\xi \qquad \cdots(10)$$

where K_β and K_ξ flapping and lag stiffness of blade.

2.2 Dynamic modelling of wing and pylon

The structural dynamic model of an elastic wing is established by using finite element discretization method[5]. As shown in Fig. 2, the three velocity components in an inertial coordinate system of the velocity $\boldsymbol{V_w}$ at a point on the cross section located at x position from the wing root are given by

$$\begin{aligned} V_{wx} &= \dot{u}_w \\ V_{wy} &= \dot{v}_w \\ V_{wz} &= \dot{w}_w + y\dot{\phi}_w \end{aligned} \qquad \cdots(11)$$

where u_w, v_w and w_w are spanwise, chordwise and vertical translational deformation of wing, respectively, and ϕ_w is the torsion of wing. y is the distance between the torsional axis of the wing and the centre of gravity of the section. The variation of virtual kinetic energy of wing is given by

$$\delta T_w = \int_0^{y_{tw}} m_w \boldsymbol{V_w} \cdot \delta \boldsymbol{V_w} \mathrm{d}x + m_p \boldsymbol{V_w} \cdot \delta \boldsymbol{V_w} \qquad \cdots(12)$$

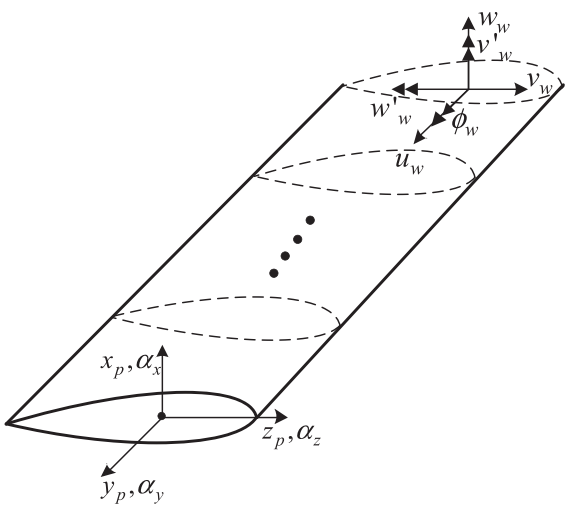

Figure 2. Structural dynamic model of wing.

https://doi.org/10.1017/aer.2018.93 Published online by Cambridge University Press

where m_w is the wing mass per unit length, m_p is the rigid pylon mass and y_{tw} is the wing length. The wing is treated as an elastic cantilever beam and modelled by using a finite element method. The variation of virtual strain energy δU_w of wing can be found in Ref. 5.

3.0 UNSTEADY AERODYNAMIC MODEL

The ONERA unsteady aerodynamic model[14,15] is used to calculate the unsteady aerodynamic forces in this paper. The aerodynamic forces components of blade aerofoil are shown in Fig. 3.

In Fig. 3, V is the airflow speed relative to the blade aerofoil, α is the angle-of-attack of the blade aerofoil, L_y and L_z are the chordwise and normal unsteady aerodynamic forces, respectively. According to the description of ONERA model[14,15], the unsteady aerodynamic forces on the aerofoil include the circulation airloads, non-circulation airloads and drag forces, where the circulation airloads can be expressed as

$$\begin{aligned} L_{yc} &= -qc\frac{w_{b0}-\lambda_{w0}}{v_{2de}}\mathrm{sgn}(v)\left[c_{l\alpha}\sin\alpha-\frac{c_{l\alpha}w_{b1}}{2v_{2de}}\right] \\ L_{zc} &= qc\frac{|v|}{v_{2de}}(c_{l\alpha}\sin\alpha) \\ M_{xc} &= \frac{1}{4}cL_{zc}\mathrm{sgn}(v) \end{aligned} \quad \cdots(13)$$

where w_{bi} $(i=0,1,2,3)$ are normal velocities caused by the blade motions and include the vertical velocities produced by flapping and pitching of the blade, and the tilting of the pylon. λ_{w0} is the normal velocity component of the unsteady dynamic induced inflow λ_w. c is the length of the blade chord, and q is the dynamic pressure. v_{2de} is the local resultant velocity of aerofoil. For rotor aerodynamic modelling, the reversed flow region cannot be neglected due to large forward flight speed in conversion flight. Therefore, it is necessary to consider the influence of blade chordwise velocity of blade on the magnitude and direction of aerodynamic forces, and terms $\mathrm{sgn}(v)$ and $|v|$ in the aerodynamic forces expressions (13) are modified by considering the effects of reversed inflow region. While the rotor is tilting, the inflow produced by forward flight perpendicular to the rotor increases, leading to greater inflow angle of the blade. Therefore, it is necessary to consider the influence of stall on lift coefficient. For different aerofoils, the lift coefficients at different angles of attack can be determined by look-up table method[16]. Since the tiltrotor aircraft can fly at a high speed, it is necessary to consider the stall effect for retreating blade and compressibility for advancing blade. According to Ref. 17, the aerodynamic model is modified by adjusting and substituting the proper lift and drag coefficients under different flight conditions in aerodynamic forces expressions.

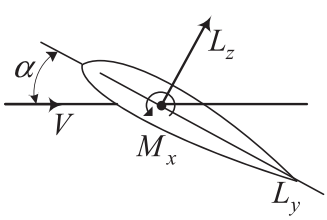

Figure 3. Aerodynamic forces components of blade aerofoil.

https://doi.org/10.1017/aer.2018.93 Published online by Cambridge University Press

The non-circulation aerodynamic forces of the aerofoil come from the airloads produced by the vibration of the aerofoil at the equilibrium position, which are given as

$$L_{znc} = \frac{1}{4}\rho c^2 \pi(\dot{w}_{b0})$$
$$M_{xnc} = -\frac{1}{64}\rho c^3 \pi(\dot{w}_{b1}) \quad \cdots(14)$$

where $\dot{w}_{b1} \approx \frac{1}{2}\mathrm{sgn}(v)c\ddot{\theta}_T$.

The drag forces of the aerofoil can be expressed by

$$L_{xd} = \frac{1}{2}\rho c c_d u v_{3d}$$
$$L_{yd} = \frac{1}{2}\rho c c_d v v_{3d}$$
$$L_{zd} = \frac{1}{2}\rho c c_d w v_{3d} \quad \cdots(15)$$

where C_d is the drag coefficients of the aerofoil. v_{3d} is the resultant velocity of the aerofoil, and is calculated by $v_{3d} = \sqrt{u^2 + v^2 + w^2}$.

The aerodynamic forces on a blade segment can be obtained by adding the circulation, non-circulation and drag aerodynamic airloads in each direction. The non-dimensional aerodynamic forces and moments on rotor shown in Fig. 1 are obtained through the following expressions:

$$\frac{M_F}{C_{l\alpha}c} = \int_0^1 r\frac{L_z}{C_{l\alpha}c}dr$$
$$\frac{M_L}{C_{l\alpha}c} = \int_0^1 r\frac{L_y}{C_{l\alpha}c}dr$$
$$\frac{C_T}{C_{l\alpha}\sigma} = \frac{1}{N_b}\sum_{i=1}^{N_b}\int_0^1 r\frac{L_z}{C_{l\alpha}c}dr$$
$$\frac{C_Q}{C_{l\alpha}\sigma} = -\frac{1}{N_b}\sum_{i=1}^{N_b}\int_0^1 r\frac{L_y}{C_{l\alpha}c}dr$$
$$\frac{C_H}{C_{l\alpha}\sigma} = \frac{1}{N_b}\sum_{i=1}^{N_b}\int_0^1 \left(\frac{L_y}{C_{l\alpha}c}\sin\psi_i + \frac{L_x}{C_{l\alpha}c}\cos\psi_i\right)dr$$
$$\frac{C_Y}{C_{l\alpha}\sigma} = \frac{1}{N_b}\sum_{i=1}^{N_b}\int_0^1 -\frac{L_y}{C_{l\alpha}c}\cos\psi_i + \frac{L_x}{C_{l\alpha}c}\sin\psi_i dr$$
$$\frac{M_x}{C_{l\alpha}c} = \frac{1}{N_b}\sum_{i=1}^{N_b}\int_0^1 r\frac{L_z\sin\psi_i}{C_{l\alpha}c}dr$$
$$\frac{M_y}{C_{l\alpha}c} = -\frac{1}{N_b}\sum_{i=1}^{N_b}\int_0^1 r\frac{L_z\cos\psi_i}{C_{l\alpha}c}dr \quad \cdots(16)$$

where M_F and M_L are the flapping and the lag aerodynamic moments, respectively. C_T, C_H and C_Y are thrust, backward force and sideward force coefficients on rotor, respectively. C_Q, M_x and M_y are torque, hub moments in the x- and the y-axis direction due to flapping motion of blades. The aerodynamic forces and moments transmitted to the wing tip can be obtained

https://doi.org/10.1017/aer.2018.93 Published online by Cambridge University Press

by the following relationships:

$$\begin{bmatrix} F_x^p \\ F_y^p \\ F_z^p \\ M_x^p \\ M_y^p \\ M_z^p \end{bmatrix} = \begin{bmatrix} \cos\alpha_p & 0 & \sin\alpha_p & 0 & 0 & 0 \\ 0 & 1 & 0 & 0 & 0 & 0 \\ -\sin\alpha_p & 0 & \cos\alpha_p & 0 & 0 & 0 \\ 0 & -h\cos\alpha_p & 0 & \cos\alpha_p & 0 & -\sin\alpha_p \\ h & 0 & 0 & 0 & 1 & 0 \\ 0 & -h\sin\alpha_p & 0 & \sin\alpha_p & 0 & \cos\alpha_p \end{bmatrix} \begin{bmatrix} C_H \\ C_Y \\ C_T \\ M_x \\ M_y \\ C_Q \end{bmatrix} \quad \cdots(17)$$

The virtual work done by external aerodynamic forces of each generalized degrees of freedom is given by

$$\delta W_b = F_x^p \delta x_p + F_y^p \delta y_p + F_z^p \delta z_p + M_x^p \delta\alpha_x + M_y^p \delta\alpha_y + M_z^p \delta\alpha_z + M_F \delta\beta + M_L \delta\xi \quad \cdots(18)$$

The aerodynamic forces of wing are obtained by strip theory, and the detailed derivation of virtual work done by aerodynamic forces of wing can be found in Ref. 5.

4.0 WAKE BENDING DYNAMIC INFLOW MODEL OF TILTROTOR

To accurately establish the induced inflow model of a tiltrotor undergoing conversion, the wake bending dynamic inflow model[12] is used. The model is based on the Peters–He generalized dynamic inflow model[8] and the modification of rotor wake bending effects. In the wake bending unsteady inflow model, the vertical induced inflow velocity on the rotor disk can be described by a series form of arbitrary order harmonics and radial shape functions

$$\lambda_w(\bar{r},\psi,t) = \sum_{r=0}^{\infty} \sum_{j=k+1,k+3,\ldots}^{\infty} \phi_j^k(\bar{r}) \left[\alpha_j^k(t)\cos(k\psi) + \beta_j^k(t)\sin(k\psi) \right] \quad \cdots(19)$$

where λ_w is the vertical induced inflow velocity on the rotor disk. α and β are the state variables of the induced inflow in the inflow model. k is the harmonic orders of induced inflow, and j is the number of shape functions. t represents time. $\bar{r}$ is the non-dimensional radius of the blade. ϕ is the radial expand function which is given as

$$\phi_j^k(\bar{r}) = \sqrt{(2j+1)H_j^k} \sum_{q=k,k+2\ldots}^{j-1} \frac{\bar{r}^q (-1)^{(q-k)/2} (j+q)!!}{(q-k)!!\,(q+k)!!\,(j-q-1)!!} \quad \cdots(20)$$

where $H_j^k = \frac{(j+k-1)!!\,(j-k-1)!!}{(j+k)!!\,(j-k)!!}$.

According to the Peters–He theoretical model, the dimensionless state equations of each cosine and sine state variable are given as,

$$\begin{aligned} \mathbf{M}_c \left\{ \alpha_j^k \right\}^{\bullet} + \mathbf{V}_c \tilde{L}_c^{-1} \left\{ \alpha_j^k \right\} &= \tau_c \\ \mathbf{M}_s \left\{ \beta_j^k \right\}^{\bullet} + \mathbf{V}_s \tilde{L}_s^{-1} \left\{ \beta_j^k \right\} &= \tau_s \end{aligned} \quad \cdots(21)$$

where $\mathbf{M}$ is the mass matrix, $\mathbf{V}$ is the mass flow parameter matrix and $\tilde{L}$ is the gain matrix relating to the skew angle-of-wake. $\boldsymbol{\tau}$ is the aerodynamic forces' coefficients on rotor disk. The subscripts c and s represent the cosine and sine terms, the analytical form of the mass

https://doi.org/10.1017/aer.2018.93 Published online by Cambridge University Press

matrix $\mathbf{M}$ is

$$\begin{bmatrix} \ddots & & \\ & \frac{2H_n^m}{\pi} & \\ & & \ddots \end{bmatrix} = \begin{cases} [\mathbf{M}_c] & m = 0, 1, 2, \ldots N \\ [\mathbf{M}_s] & m = 1, 2, 3, \ldots N \end{cases} \quad \cdots(22)$$

The cosine and the sine part of the gain matrix are $[\tilde{\mathbf{L}}_c] = \begin{bmatrix} \vdots & \cdots\vdots \\ \tilde{L}_{jn}^{kmc} & \end{bmatrix}$ and $[\tilde{\mathbf{L}}_s] = \begin{bmatrix} \cdots & \vdots & \cdots \\ & [\tilde{L}_{jn}^{kms}] & \\ & \vdots & \end{bmatrix}$ respectively, where

$$\begin{aligned} \left[\tilde{L}_{jn}^{0m}\right]^C &= X^m \left[\Gamma_{jn}^{0m}\right] \\ \left[\tilde{L}_{jn}^{rm}\right]^C &= \left[X^{|m-k|} + (-1)^l X^{|m+k|}\right] \left[\Gamma_{jn}^{km}\right] \\ \left[\tilde{L}_{jn}^{km}\right]^S &= \left[X^{|m-k|} - (-1)^l X^{|m+k|}\right] \left[\Gamma_{jn}^{km}\right] \end{aligned} \quad \cdots(23)$$

where $l = \min(k, m)$, $X = \tan|\chi/2|$, and if $k+m$ is even, $\Gamma_{jn}^{km} = \frac{(-1)^{\frac{n+j-2k}{2}} \cdot 2\sqrt{(2n+1)(2j+1)}}{\sqrt{H_n^m H_j^k (n+j)(n+j+2)[(n-j)^2-1]}}$; if $k+m$ is odd and $j = n \pm 1$, $\Gamma_{jn}^{km} = \frac{\pi \cdot \mathrm{sgn}(k-m)}{2\sqrt{H_n^m H_j^k (2n+1)(2j+1)}}$; if $k+m$ is odd and $j \neq n \pm 1$, $\Gamma_{jn}^{rm} = 0$.

In above expressions, $\chi = \pi/2 - \alpha_w$, where α_w is the skew angle-of-wake, defined as

$$\alpha_w = \tan^{-1}\left(\frac{\lambda_0 + \overline{V_c}}{V \cos\alpha_p}\right) \quad \cdots(24)$$

where λ_0 is the steady term of the axial inflow. $\overline{V_c}$ is the dimensionless velocity components of flight inflow perpendicular to the rotor plane, respectively.

The mass flow parameter matrix $\boldsymbol{V}$ includes $\boldsymbol{V_c} = \begin{bmatrix} V_m & \\ & \overline{V} \end{bmatrix}$ and $\boldsymbol{V_s} = [\overline{V}]$, where V_m is the parameter associated with the time average inflow, given as $V_m = \sqrt{\mu^2 + (\lambda_0 + \overline{V_c})^2}$ and $\overline{V}$ is the high order mass flow parameter, defined as $\overline{V} = [\mu^2 + (\lambda_0 + \overline{V_c})(2\lambda_0 + \overline{V_c})] / V_m$.

In conversion flight, the incoming airstream does not generally flow perpendicular (through the disk). Also, the pylon is simultaneously tilting, which makes the wake bending occur simultaneously with the tilting of the rotor. According to the vortex tube theory model[18] and considering the rotor wake bending effects, the state equations for each inflow variable are written as

$$\begin{aligned} \mathbf{M}_c \left\{\alpha_j^k\right\}^{\bullet} + \mathbf{V}_c \tilde{L'}_c^{-1} \left\{\alpha_j^k\right\} &= \tau_c \\ \mathbf{M}_s \left\{\beta_j^k\right\}^{\bullet} + \mathbf{V}_s \tilde{L'}_s^{-1} \left\{\beta_j^k\right\} &= \tau_s \end{aligned} \quad \cdots(25)$$

where the cosine part $\tilde{L'}_c$ and sine part $\tilde{L'}_s$ of gain matrix are,

$$\begin{aligned} \tilde{L'}_c &= \tilde{L}_c + \mathbf{C}_{pk} \kappa_c \\ \tilde{L'}_s &= \tilde{L}_s + \mathbf{C}_{pk} \kappa_s \end{aligned} \quad \cdots(26)$$

where $\mathbf{C}_{pk}$ is the inflow coupling parameter matrix of wake bending. κ_c and κ_s are the

https://doi.org/10.1017/aer.2018.93 Published online by Cambridge University Press

longitudinal and lateral bending coefficients of wake, which are

$$\kappa_c = \frac{q_h - \dot{\beta}_{1c}}{\lambda_0 + \overline{V}_c}$$
$$\kappa_s = \frac{p_h - \dot{\beta}_{1s}}{\lambda_0 + \overline{V}_c} \quad \cdots(27)$$

where q_h and p_h are the longitudinal and the lateral tilting angular velocity of rotor shaft, respectively. $\dot{\beta}_{1c}$ and $\dot{\beta}_{1s}$ are the longitudinal and lateral angular velocity of the flapping motion of the rotor disk respectively.

The above detailed derivation can be found in Ref. 12.

5.0 ASSEMBLING OF ROTOR/PYLON/WING DYNAMIC MODELS

Substituting the above derived virtual kinetic, strain energy and work expressions into Equation (1) and combining the terms with identical variables, the following expression in matrix form can be obtained

$$\mathbf{M}_1\ddot{q} + \mathbf{C}_1\dot{q} + \mathbf{K}_1\mathbf{q} = \mathbf{F} \quad \cdots(28)$$

where the column vector q contains the rotor, wing and inflow variables, which is

$$\boldsymbol{q} = \{\beta, \xi, x_p, y_p, z_p, \alpha_x, \alpha_y, \alpha_z, u_w^1, w_w^1, v_w^1, \phi_w^1, v_w'1, w_w'1, \ \ldots \ , u_w^n, w_w^n, v_w^n, \phi_w^n, v_w'n, w_w'n, \alpha_j^k, \beta_j^k\}^T$$

As shown in Fig. 2, the rotor is coupled with the pylon/wing system by six degrees of freedom between the hub and wing tip. Without considering of the wing sweep angle, the transformation relationship between the wing tip degrees of freedom and elastic beam degrees of freedom of wing is given by

$$\begin{bmatrix} x_p \\ y_p \\ z_p \\ \alpha_x \\ \alpha_y \\ \alpha_z \end{bmatrix} = \begin{bmatrix} \cos\alpha_p & 0 & -\sin\alpha_p & 0 & 0 & 0 \\ 0 & 1 & 0 & 0 & 0 & 0 \\ \sin\alpha_p & 0 & \cos\alpha_p & 0 & 0 & 0 \\ 0 & 0 & 0 & \cos\alpha_p & 0 & -\sin\alpha_p \\ 0 & 0 & 0 & 0 & 1 & 0 \\ 0 & 0 & 0 & \sin\alpha_p & 0 & \cos\alpha_p \end{bmatrix} \begin{bmatrix} 0 & 1 & 0 & h & 0 & 0 \\ 1 & 0 & 0 & 0 & -h & 0 \\ 0 & 0 & 1 & 0 & 0 & 0 \\ 0 & 0 & 0 & 0 & 1 & 0 \\ 0 & 0 & 0 & 1 & 0 & 0 \\ 0 & 0 & 0 & 0 & 0 & 1 \end{bmatrix} \begin{bmatrix} u_{tip} \\ w_{tip} \\ v_{tip} \\ \phi_{tip} \\ v'_{tip} \\ w'_{tip} \end{bmatrix} \quad \cdots(29)$$

The differential equations of tiltrotor aircraft in conversion flight can be obtained by substituting and assembling Equation (29), the Fourier transformation expressions (6) and (7) into Equation (28), and combing with the inflow state equations (25)

$$M\ddot{\mathbf{x}} + \mathbf{C}(\psi)\dot{\mathbf{x}} + \mathbf{K}(\psi)\mathbf{x} = \mathbf{F} \quad \cdots(30)$$

where **M**, **C** and **K** are the mass, damping and stiffness matrices of the system, respectively, and the damping and stiffness matrices are varied with the blade azimuth angle. x is the column vector consisting of the system variables. In this paper, taking articulated rotor with three blades, discretizing the elastic wing into six finite element nodes, adopting two harmonics of induced flow ($r = 2$) and three shape functions for each harmonic ($j = 3$), the vector

https://doi.org/10.1017/aer.2018.93 Published online by Cambridge University Press

x is defined as

$$\boldsymbol{x} = \{\boldsymbol{x_r}, \boldsymbol{x_w}, \boldsymbol{x_\lambda}\}^T = \{\beta_0, \beta_{1c}, \beta_{1s}, \xi_0, \xi_{1c}, \xi_{1s}, u_w^1, v_w^1, \phi_w^1, v_w'^1, w_w'^1, \ \cdots\ ,$$
$$u_w^6, v_w^6, \phi_w^6, v_w'6, w_w'6, \alpha_1^0, \alpha_3^0, \alpha_5^0, \quad \alpha_2^1, \alpha_4^1, \alpha_6^1, \alpha_3^2, \alpha_5^2, \alpha_7^2, \beta_2^1, \beta_4^1, \beta_6^1, \beta_3^2, \beta_5^2, \beta_7^2\}^T$$

The size of coefficients matrices in Equation (30) is 51×51. The right side $\boldsymbol{F}$ of Equation (30) includes the external aerodynamic force terms, non-linear terms and constant terms independent of variables.

6.0 SOLUTION FOR AEROELASTIC STABILITY

6.1 Trim calculation

The trim calculation of the tiltrotor aircraft in conversion flight was carried out by the wind tunnel trim method[16]. First, the flight condition is determined by the given tilt angle of the pylon and the forward speed. The trim control inputs are determined by calculating the response of each pitch input with time at specified lift coefficient of rotor[19]. The coefficient terms related to trim control inputs θ_0, θ_c and θ_s are moved to the left side in Equation (30), and the trim control equations are introduced as

$$\begin{bmatrix} \tau_0 & 0 & 0 \\ 0 & \tau_1 & 0 \\ 0 & 0 & \tau_1 \end{bmatrix} \begin{pmatrix} \theta_0 \\ \theta_s \\ \theta_c \end{pmatrix}^{\cdot\cdot} + \begin{pmatrix} \theta_0 \\ \theta_s \\ \theta_c \end{pmatrix}^{\cdot} = \begin{bmatrix} K_0 & 0 & 0 \\ 0 & K_1 & 0 \\ 0 & 0 & K_1 \end{bmatrix} \begin{bmatrix} \frac{6}{C_{l\alpha}} & 0 & 0 \\ 0 & \frac{8\left(v_\beta^2 - 1\right)}{\gamma} & -1 \\ 0 & 1 & \frac{8(v_\beta^2 - 1)}{\gamma} \end{bmatrix} \begin{bmatrix} \overline{C_T} - C_T \\ \overline{\beta_s} - \beta_s \\ \overline{\beta_c} - \beta_c \end{bmatrix} \quad \cdots(31)$$

where τ_0, τ_1, K_0 and K_1 are parameters controlling the convergence speed of the trim calculation. $\overline{C_T}$, $\overline{\beta_c}$ and $\overline{\beta_s}$ are objective values of trim parameters. The trim control dynamic equation is obtained by combing Equations (30) and (31)

$$\mathbf{M}_c \ddot{x}_c + \mathbf{C}_c \dot{x}_c + \mathbf{K}_c x_c = \mathbf{F}_c \quad \cdots(32)$$

where $x_{\boldsymbol{c}} = \{x_r, x_w, x_\lambda, x_\theta\}^{\mathrm{T}}$ and $x_\theta = \{\theta_0, \theta_c, \theta_s\}^{\mathrm{T}}$, in which θ_0 is the collective pitch, θ_c and θ_s are the longitudinal and the lateral cyclic pitch, respectively. The trim control inputs are determined by calculating the responses of Equation (32) at zero initial conditions, and the responses of each variable are obtained by calculating the response of Equation (30) with the trimmed inputs.

6.2 Linearization of nonlinear equations

The nonlinear terms at the right side of Equation (30) need to be linearized about a trim point to facilitate the solution procedure for stability analysis. Unsteady aerodynamic forces produce oscillations about the equilibrium position of aerofoil in conversion flight. The small perturbation assumption method is used here, and each variable can be treated as small perturbation about the trimmed values, which are written as

$$\begin{aligned} \mathbf{x}_R &= \mathbf{x}_{R0} + \Delta\mathbf{x}_R \\ \mathbf{x}_w &= \mathbf{x}_{w0} + \Delta\mathbf{x}_w \\ \mathbf{x}_\lambda &= \mathbf{x}_{\lambda 0} + \Delta\mathbf{x}_\lambda \end{aligned} \quad \cdots(33)$$

https://doi.org/10.1017/aer.2018.93 Published online by Cambridge University Press

The dynamic equations for aeroelastic stability analysis of tiltrotor can be obtained by substituting the expression (33) into Equation (30), and eliminating the higher order perturbation terms, which are

$$\mathbf{M}\Delta\ddot{\mathbf{x}} + \mathbf{C}_0(\psi)\Delta\dot{\mathbf{x}} + \mathbf{K}_0(\psi)\Delta\mathbf{x} = 0 \quad \cdots(34)$$

where $\mathbf{C}_0$ and $\mathbf{K}_0$ are linearized damping and stiffness matrices.

6.3 Stability solution

In conversion flight, the damping and stiffness matrices in Equation (34) vary periodically with blade azimuth angle, and the matrices satisfy the relations

$$\begin{aligned}\mathbf{C}_0(\psi_0) &= \mathbf{C}_0(\psi_0 + 2\pi)\\ \mathbf{K}_0(\psi_0) &= \mathbf{K}_0(\psi_0 + 2\pi)\end{aligned} \quad \cdots(35)$$

The stability analysis of dynamic equations with periodic coefficients is carried out by using Floquet theory, and Equation (34) is transformed into a first-order differential equation in the state space, which is

$$\dot{Y} = \mathbf{A}(\psi)Y \quad \cdots(36)$$

where $Y = \{\Delta x_R, \Delta\dot{x}_R, \Delta x_W, \Delta\dot{x}_W, \Delta x_\lambda\}$, and $\mathbf{A}(\psi)$ is the state matrix consisting of periodic coefficients. According to Floquet theory, the transition matrix $[\Phi(t, t_0)]$ is obtained by using

Table 1
Main parameters of rotor and wing

Rotor parameters	**Value**
Number of blades, N_b	3
Rotor radius, R/m	3.82
Lock number γ	3.83
Rotor solidity, σ	0.089
Rotational speed Ω/rad/s	48
Flap coupling coefficient, K_p	−0.268
Static lift curve slope of blade, C_{la}/rad^{-1}	5.7
Inertial moment of flapping I_b/kg·m^2	142
Linear negative twist of blade θ_{tw}/°	−41
Wing/pylon parameters	Value
wing length y_{tw}/m	5.09
Structural stiffness of wing	
K_{q1}/(N/m)	9.2×10^6
K_{q2}/(N/m)	2.5×10^7
K_p/(N·m/rad)	1.8×10^6
Structural damping of wing	
C_{q1}/(N·s/m)	9,030
Cq^2/(*N·s/m*)	27,300
C_p/(N·m·s/rad)	955
Pylon length, h/m	1.31
Inertial moment of pylon, m_p/kg m^2	16,380

https://doi.org/10.1017/aer.2018.93 Published online by Cambridge University Press

the fourth-order Runge–Kutta method to calculate the total response of Equation (36) over one time period. The eigenvalues and eigenvectors of $[\Phi(t, t_0)]$ at the end point of one time period ($t = t_0 + 2\pi$) are also obtained. The negative real parts of the eigenvalues are the modal damping, and the system is unstable if any modal damping is less than 0.

7.0 STABILITY ANALYSIS OF TILTROTOR AIRCRAFT

The test model parameters of a tiltrotor aircraft[17] are used as the baseline study in this paper, and the main parameters of rotor and wing are listed in Table 1.

7.1 Trim analysis of tiltrotor aircraft

The variation of the tilt angle-of-pylon with time is shown in Fig. 4. In the first 2 s, the rotor is trimmed in helicopter flight mode, and no wake bending occurs since the pylon does not tilt. The pylon tilts from the second seconds to the 7th seconds at a constant angular velocity of

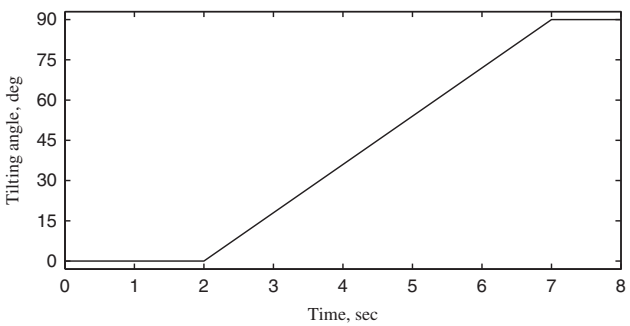

Figure 4. Tilt angle-of-pylon α_p changing with time.

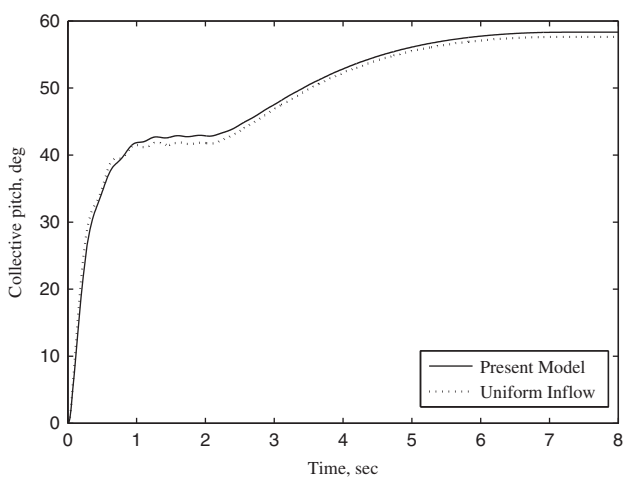

Figure 5. Collective pitch θ_0 changing with time ($V/\Omega R = 0.3$).

https://doi.org/10.1017/aer.2018.93 Published online by Cambridge University Press

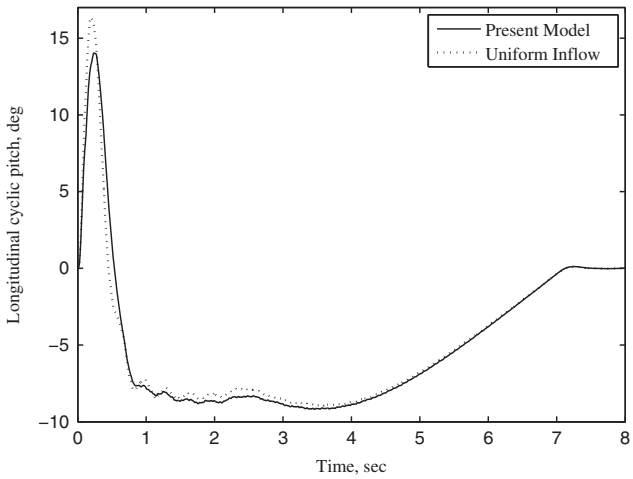

Figure 6. Longitudinal cyclic pitch θ_s changing with time ($V/\Omega R = 0.3$).

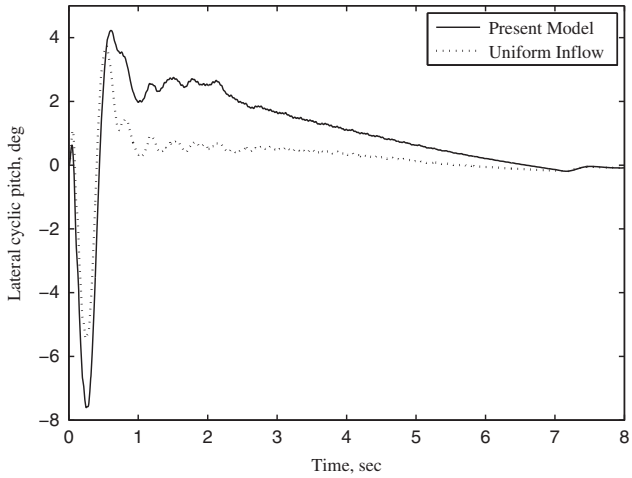

Figure 7. Lateral cyclic pitch θ_c changing with time ($V/\Omega R = 0.3$).

18° per second. The tilt angle of the pylon becomes 90° at the end of the seventh second, with the tiltrotor aircraft entering into aircraft flight mode and achieving an axial flow condition. According to the parameters listed in Table 1, the transient responses of collective θ_0 and cyclic pitch θ_c, θ_s for rotor trim with time at different forward speeds are calculated when the pylon tilts continuously. The calculated results using wake bending unsteady dynamic inflow are compared with a uniform inflow assumption, as shown in Figs 5–10. In particular, Figs 5–7 show the variation of trimmed pitch values with time for a forward speed 0.3 and Figs 8–10 show a forward speed of 0.5. Together, these figures show that while the pylon tilts forward and the tiltrotor aircraft converts from the helicopter flight mode to aircraft flight mode, the velocity component of forward velocity along the rotor shaft direction increases, leading to an increase in the inflow angle of the blade section. Hence, the collective pitch is increased to manage the thrust. During the forward tilting of the pylon, the bending inflow

https://doi.org/10.1017/aer.2018.93 Published online by Cambridge University Press

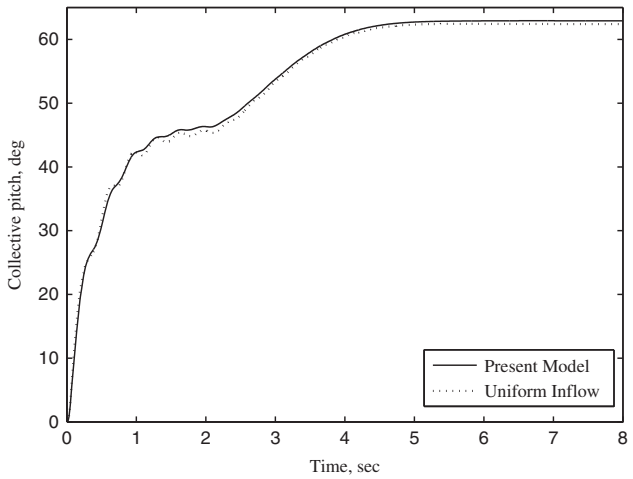

Figure 8. Collective pitch θ_0 changing with time ($V/\Omega R = 0.5$).

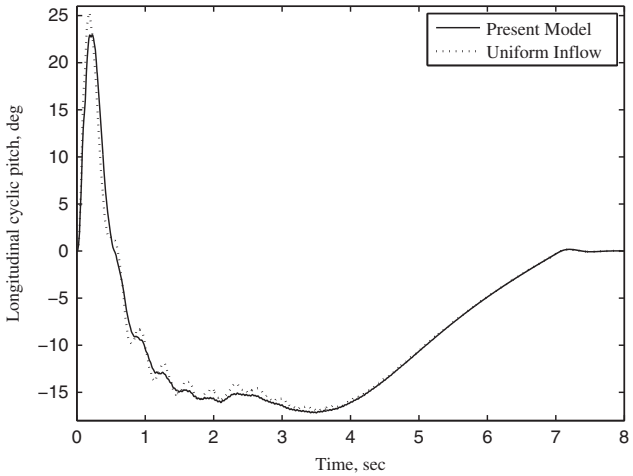

Figure 9. Longitudinal cyclic pitch θ_s changing with time ($V/\Omega R = 0.5$).

distribution in conversion flight becomes a symmetric distribution in aircraft flight, and the cyclic pitch eventually becomes 0 in aircraft flight mode. The difference in trimmed control inputs between the assumptions of allowing wake bending unsteady dynamic inflow compared with the uniform inflow assumption is mainly seen in the lateral cyclic pitch θ_c, indicating that the bending wake unsteady dynamic inflow is mainly trimmed by lateral cyclic pitch while the pylon is tilting. As the pylon tilts forward and the forward speed increases, the forward velocity component along the rotor shaft direction increases, becoming much larger than the unsteady induced inflow in magnitude, and the influence of wake bending unsteady dynamic inflow on the control inputs gradually reduces.

https://doi.org/10.1017/aer.2018.93 Published online by Cambridge University Press

7.2 Stability analysis of tiltrotor aircraft in conversion flight

The non-linear dynamic equations were linearized on the basis of the steady response of each variable by using trimmed control inputs, and the stability analysis of tiltrotor aircraft in conversion flight was conducted in this paper. According to Ref. 20, the tiltrotor aircraft usually enters into the conversion flight at the forward speed between 0.3 and 0.5. Therefore, the stability analysis is investigated by calculating the variations of modal damping with the tilt angle-of-pylon at the forward speed of 0.3 and 0.5, respectively, which are shown in Figs 11–16. The terms p, q_1 and q_2 represent, respectively, the first

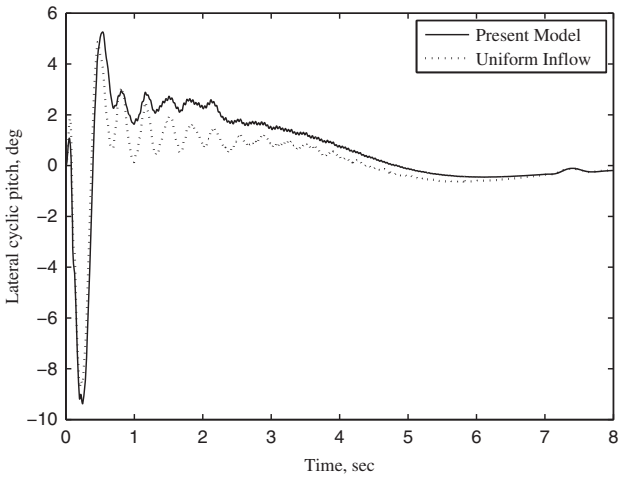

Figure 10. Lateral cyclic pitch θ_c changing with time ($V/\Omega R = 0.5$).

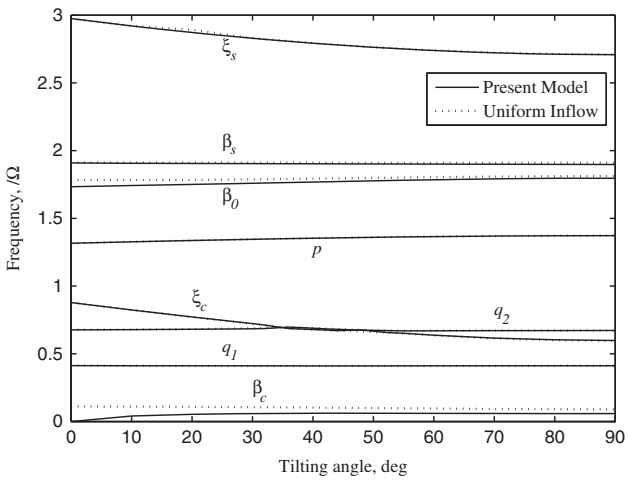

Figure 11. Frequencies of rotor and wing modes changing with tilt angle-of-pylon ($V/\Omega R = 0.3$).

https://doi.org/10.1017/aer.2018.93 Published online by Cambridge University Press

order torsional, vertical bending and chordwise bending modes of the wing. It can be seen from Figs 11–14, when the pylon tilts forward, more collective pitch is needed for trimming, which aggravates the structural coupling between flapping and lag of blade, leading a decrease in the frequencies of lag modes ξ_s, ξ_c and a slight increase in the frequencies of flapping modes β_0, β_c, β_s, and the changing in frequencies of flapping and lag modes with tilt angle become more obvious as the forward speed increases. The unsteady wake bending dynamic inflow produces a slight influence on the frequencies of the blade flapping modes, but has little influence on the frequencies of lag modes and wing modes. As shown in Figs 12–15, the damping of flapping modes reduces with the consideration of the wake bending unsteady dynamic inflow, indicating that the unsteady inflow has sig-

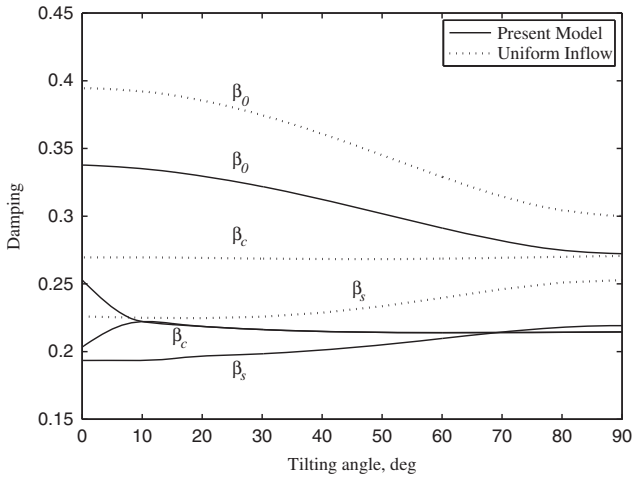

Figure 12. Damping of flapping modes changing with tilt angle-of-pylon ($V/\Omega R = 0.3$).

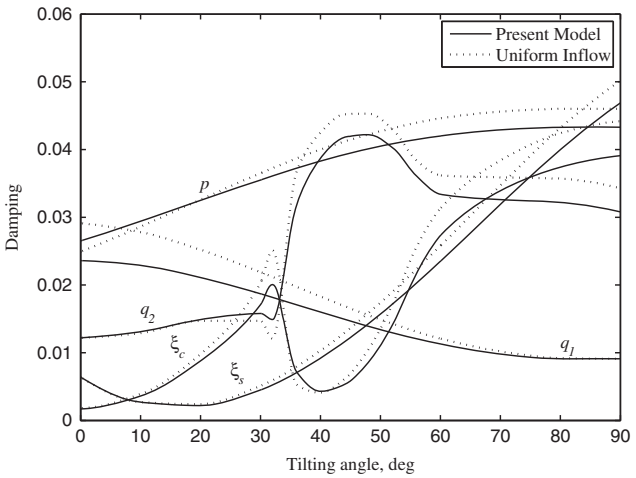

Figure 13. Damping of lag and wing modes changing with tilt angle-of-pylon ($V/\Omega R = 0.3$).

https://doi.org/10.1017/aer.2018.93 Published online by Cambridge University Press

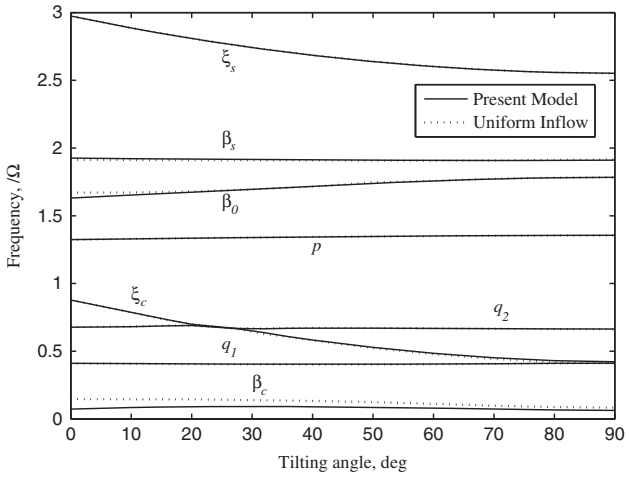

Figure 14 . Frequencies of rotor and wing modes changing with tilt angle-of-pylon ($V/\Omega R = 0.5$).

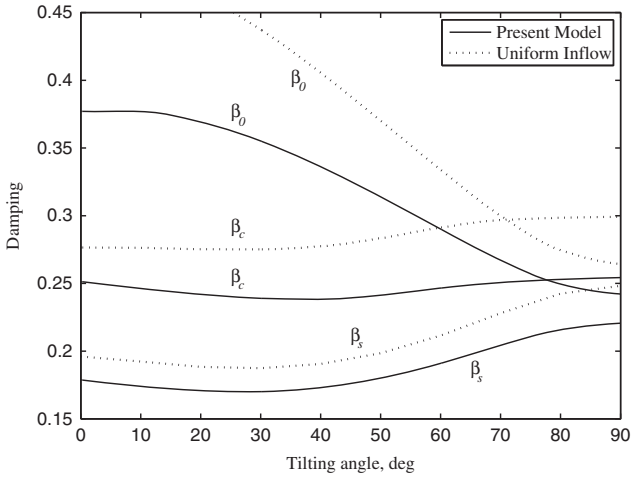

Figure 15. Damping of flapping modes changing with tilt angle-of-pylon ($V/\Omega R = 0.5$).

nificant influence on rotor lift. It can be seen in Figs 13–16, that while the pylon is in motion, tilting to horizontal and forward, which makes damping of the wing first vertical bending mode q_1 less and while increasing the damping of the wing first chordwise bending mode q_2 with the forward tilting of pylon. When the frequency of ξ_c and q_2 approaches, abrupt changes of corresponding modal damping occur. When the forward speed is 0.5, the damping of the wing first chordwise bending mode q_2 is negative as the pylon tilts about 23°, making the wing first chordwise bending mode q_2 unstable. Since the aerodynamic forces of rotor and wing increase with the increase of forward speed, the coupling between the modes makes the instability more prone to occur at higher forward speed for the given conditions.

https://doi.org/10.1017/aer.2018.93 Published online by Cambridge University Press

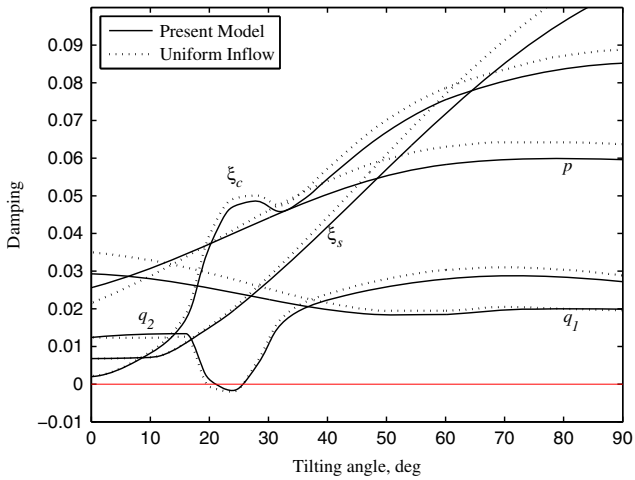

Figure 16. Damping of lag modes and wing bending modes changing with tilt angle-of-pylon ($V/\Omega R = 0.5$).

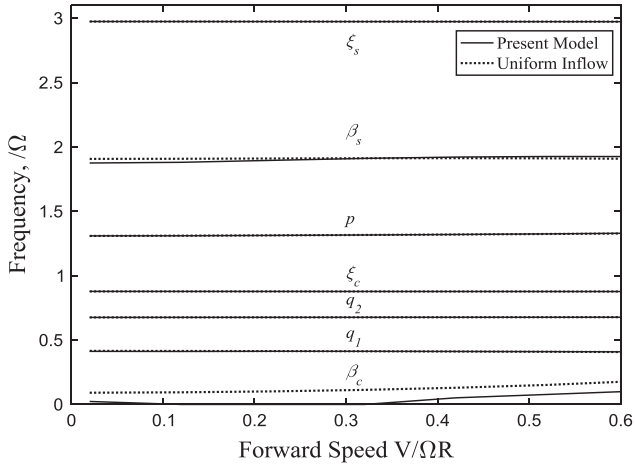

Figure 17. Frequencies of rotor and wing modes changing with forward speed ($\alpha_p = 0°$).

According to the above analysis, the system instability is mainly due to the coupling between the lag modes of the rotor and the bending/torsional modes of the wing. To analyse the aeroelasticity of tiltrotor aircraft at different tilt angles, the variations of each cyclic lag and wing modal frequency and damping with forward flight speed at different tilt angle-of-pylon are calculated and plotted in Figs 17–24, in which the calculations without wake bending dynamic inflow assumption are also shown for comparison. From Figs 17–22, the figures show the helicopter flight mode and the conversion flight mode in which the shown maximum forward speeds are $V/\Omega R = 0.6$. Figures 23 and 24 show the turboprop aircraft flight mode in which the shown maximum forward speeds are $V/\Omega R = 1.5$. It can be seen from Fig. 17 that the tilt angle-of-pylon is 0° for helicopter flight, where the pylon does not tilt and no wake bending effect on rotor occurs. The frequency of β_c mode gradually

https://doi.org/10.1017/aer.2018.93 Published online by Cambridge University Press

increases at a high forward speed due to the rotor pitch/flap coupling coefficient. The aerodynamic forces on the rotor plane increase as the forward speed increases, in which the thrust perpendicular to the rotor plane increases, leading to an increase on the damping of the wing first vertical bending mode q_1, and aerodynamic moments produced by the forces parallel to the rotor plane increase, leading to a decrease on the damping of the wing first torsional mode p. According to the above analysis, the wake bending dynamic inflow reduces the aerodynamic forces on the rotor plane, which causes a decrease in the damping of the wing first vertical bending mode q_1 and an increase in the damping of the wing first torsional mode p.

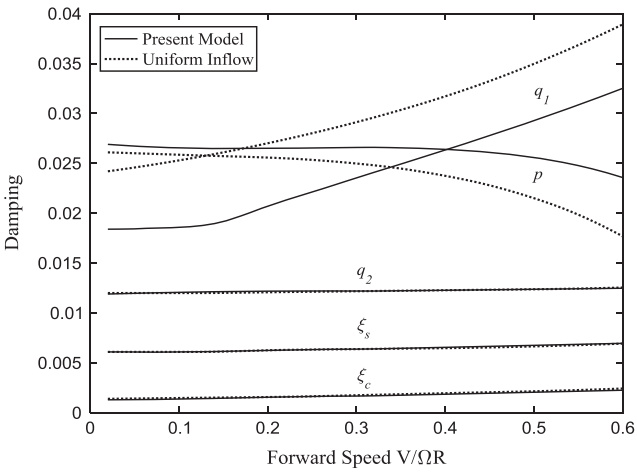

Figure 18. Damping of lag and wing modes changing with forward speed ($\alpha_p = 0°$).

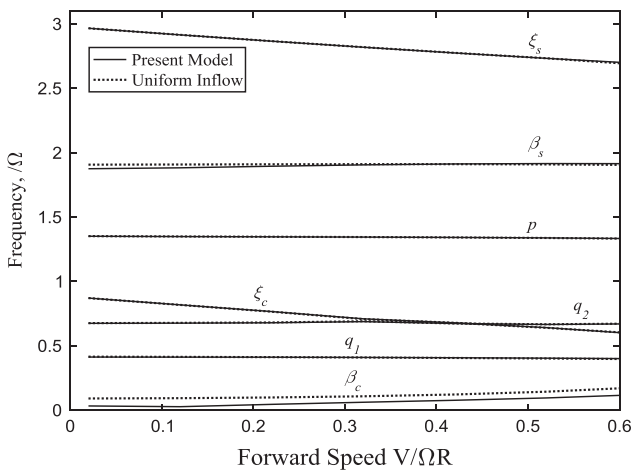

Figure 19. Frequencies of rotor and wing modes changing with forward speed ($\alpha_p = 30°$).

https://doi.org/10.1017/aer.2018.93 Published online by Cambridge University Press

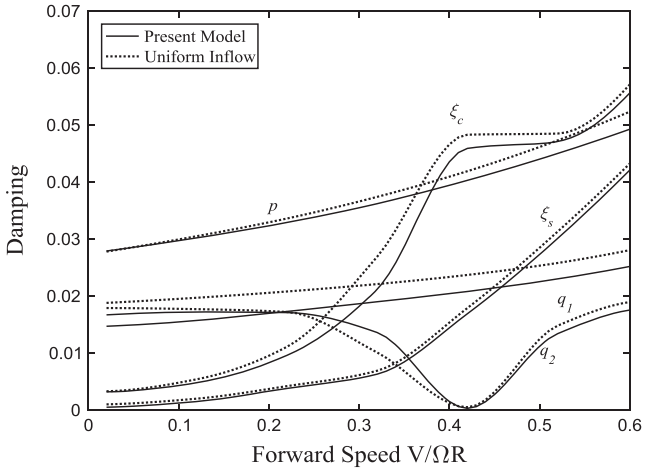

Figure 20. Damping of lag and wing modes changing with forward speed ($\alpha_p = 30°$).

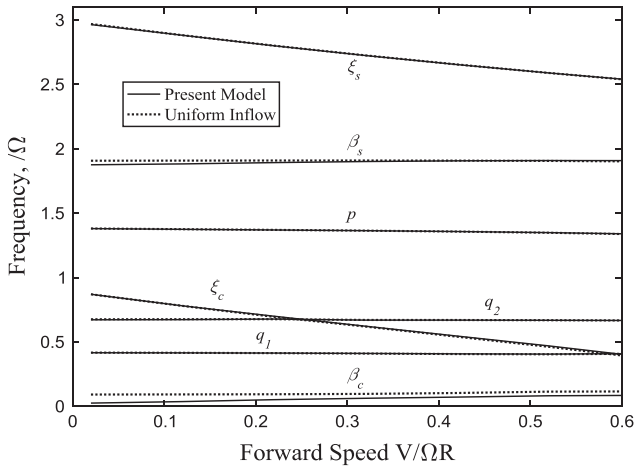

Figure 21. Frequencies of lag and wing modes changing with forward speed ($\alpha_p = 60°$).

The variations of each modal frequency and damping with forward flight speed in conversion flight are plotted in Figs 19–22. It can be seen that the forward tilting motion of pylon causes the frequencies of lag modes to decrease as the forward velocity increases. When the frequency of ξ_c is close to the frequency of the wing first vertical bending mode q_1 and chordwise bending mode q_2, a sudden change in damping for corresponding modes and obvious couplings between the modes appear. This can be seen in Fig. 20, when the tilt angle-of-pylon is 30° and the forward speed is 0.41, the damping of the wing first chordwise bending mode q_2 is very close to 0. Since the component of forward velocity along the rotor shaft direction is much greater than unsteady induced inflow in high-speed flight, the influence of wake bending dynamic inflow on the system stability becomes insignificant.

https://doi.org/10.1017/aer.2018.93 Published online by Cambridge University Press

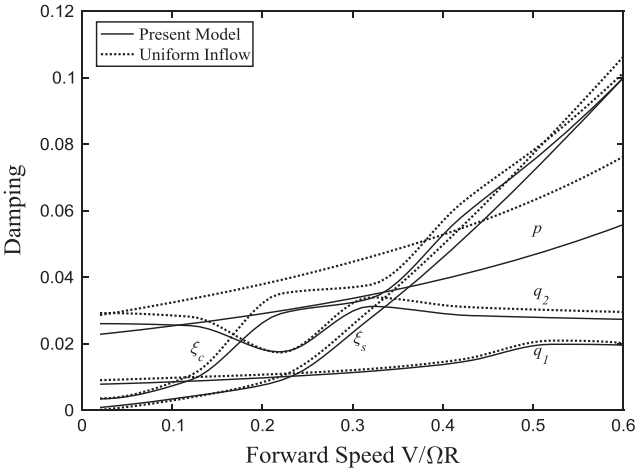

Figure 22. Damping of lag and wing modes changing with forward speed ($\alpha_p = 60°$).

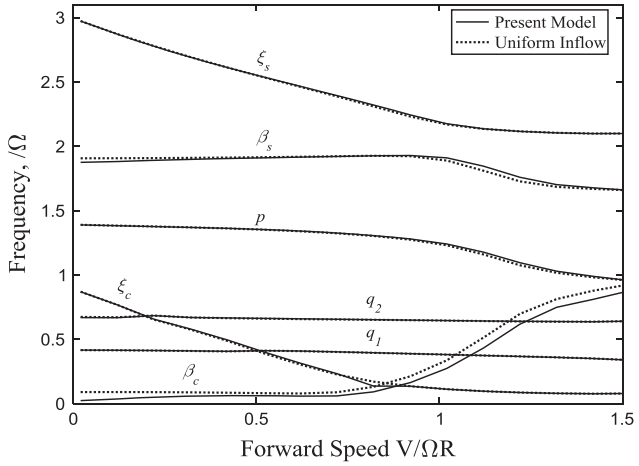

Figure 23. Frequencies of rotor and wing modes changing with forward speed ($\alpha_p = 90°$).

When the tilt angle-of-pylon is 90°, the tiltrotor aircraft is in turboprop aircraft flight mode. In this case, the rotor is in axial flight and no wake bending occurs. The variations of each modal frequency and damping with forward flight speed are plotted in Figs 23 and 24. It can be seen from Fig. 24 that the component of forward velocity along the rotor shaft direction is much greater than wake bending unsteady dynamic inflow, thus the influence of dynamic inflow is not obvious. The damping of the wing first vertical bending mode q_1 is less than 0 and the system is unstable at the forward speed 1.12. The instability form is the divergent vertical motion of wing tip, which is consistent with stability analysis in forward flight[5].

https://doi.org/10.1017/aer.2018.93 Published online by Cambridge University Press

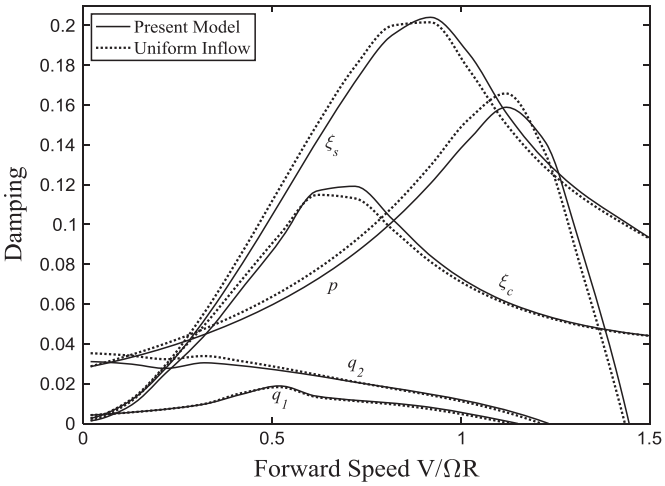

Figure 24. Damping of lag and wing modes changing with forward speed ($\alpha_p = 90°$).

8.0 CONCLUSION

In this paper, an aeroelastic stability analysis model for a tiltrotor aircraft in conversion flight has been proposed by using a rotor wake bending model, an unsteady dynamic inflow model, an unsteady aerodynamic model, and the structural coupling of rotor/pylon/wing. The results indicate that (1) compared with the uniform inflow model, the unsteady wake bending dynamic inflow is mainly trimmed by lateral cyclic pitch θ_c; (2) the unsteady wake bending dynamic inflow has significant influence on rotor flapping modes, decreasing the damping of each flapping mode, and the influence of unsteady inflow on lag and wing modes is insignificant; (3) in conversion flight, when the pylon tilts at a high forward speed, the instability occurs in chordwise bending mode of wing; (4) in turboprop aircraft flight mode, the unsteady wake bending dynamic inflow has little influence on the stability of tiltrotor aircraft in forward flight.

REFERENCES

1. KIM, T. Advanced analysis on tiltrotor aircraft flutter stability, including unsteady aerodynamics, *AIAA J*, 2015, **46**,(4), pp 1002-1012.
2. KAZA, K. Effects of steady coning angle and damping on whirl flutter stability, *J Aircr*, 2015, **10**, (11), pp 664-6693
3. SINGH, R., GANDHI, F. and PAIK, J. Active tiltrotor whirl-flutter stability augmentation using wing-flaperon and swash-plate actuation, *J Aircr*, 2015, **44**, (5) pp 1439-1446.
4. ZHANG, J. and SMITH, E.C. Influence of aeroelasticity tailored wing extensions and winglets on whirl flutter stability, 2nd Asian Rotorcraft Forum, Tianjin, China, 2013, pp 188-200.
5. NIXON, M.W. Aeroelastic Response and Stability of Tiltrotors with Elastically-coupled Composite Rotor Blades, Ph.D. thesis, University of Maryland, 1994.
6. SLABY, J. and SMITH, E. Aeroelastic stability of folding tiltrotor aircraft in cruise flight with composite wings, 52nd AIAA/ASME/ASCE/AHS/ASC Structures, Structural Dynamics and Materials Conference, Denver, Colorado, 2011, pp 2171-2179.
7. KIM, T., LIM, J. and SHIN, S.J. Structural design optimization of a tiltrotor aircraft composite wing to enhance whirl flutter stability, *Composite Structures*, 2013, **95**, (1), pp 283-194.

https://doi.org/10.1017/aer.2018.93 Published online by Cambridge University Press

8. HE, C.J. Development and Application of Generalized Dynamic Wake Theory for Lifting Rotors, PhD Thesis, Georgia Institute of Technology, 1989.
9. VENKATESAN, C. Effects of blade configuration parameters on helicopter rotor structural dynamics and whirl tower loads, *Aeronautics J*, 2016, **120**, (1224), pp 271-290.
10. KUMAR, M. and VENKATESAN, C. Effects of blade-tip geometry on helicopter trim and control response *Aeronautics J – New Series*, 2017, pp 1-23.
11. KROTHAPALLIK, R., PRASAD, J.V. and PETERS, D.A. Helicopter rotor dynamic inflow modeling for maneuvering, *J of the American Helicopter Soc*, 2001, **46**, (2), pp 129-139.
12. YUE, H.L. and XIA, P.Q. A wake bending unsteady dynamic inflow model of tiltrotor in conversion flight of tiltrotor aircraft, *Science in China Series E-Technological Sciences*, 2009, **52**, (11) pp 3188-3197.
13. LI, Z.Q. and XIA, P.Q. Whirl Flutter and Rotor Hub Center's Motion Image of Tiltrotor Aircraft, the 7th Asia Pacific International Symposium on Aerospace Technology, Cairns, Australia, 2015.
14. BERTIN, J. and SMITH, ML. *Incompressible Flow About Wings of Finite Span, Aerodynamics for Engineers*. 3rd ed. Prentice-Hall, Upper Saddle River, NJ, 1998, pp 261-336.
15. SAFFMAN, P.G. *Vortex Force and Bound Vorticity, Vortex Dynamics*, Cambridge University Press, New York, USA, 1992, pp 46-48.
16. JOHNSON, W. *Helicopter Theory*, Dover Publication, US, 1994, pp 196-198.
17. JOHNSON, W. Dynamics of Tilting Proprotor Aircraft in Cruise Flight, Technical Report, NASA/TN D-7677, 1974.
18. KELLER, J.D. An investigation of helicopter dynamic coupling using an analytical model, *J of American Helicopter Soc*, 1996, **41**, (4), pp 322-330.
19. PETERS, D.A., KIM, B.S. and CHEN, H.S. Calculation of trim settings for a helicopter rotor by an optimized controller, *J Guidance, Control and Dynamics*, 1984, **7**, (1), pp 85-97.
20. WERNICKE, G. Performance and Safety Aspects of the XV-15 Tilt Rotor Research Aircraft, 33rd AHS Annual National Form, Washington, DC, USA, 1977.

https://doi.org/10.1017/aer.2018.93 Published online by Cambridge University Press